Journal of Power Sources 194 (2009) 38–44

Contents lists available at ScienceDirect

Journal of Power Sources

journal homepage: www.elsevier.com/locate/jpowsour

Structural and transport properties of layered $Li_{1+x}(Mn_{1/3}Co_{1/3}Ni_{1/3})_{1-x}O_2$ oxides prepared by a soft chemistry method

Makoto Gozu [a], Konrad Świerczek [b,*], Janina Molenda [b]

[a] Faculty of Engineering, Shibaura Institute of Technology, 3–7–5 Toyosu, 135–8548, Koto-ku, Tokyo, Japan
[b] Faculty of Materials Science and Ceramics, AGH University of Science and Technology, al. Mickiewicza 30, 30 – 059 Kraków, Poland

ARTICLE INFO

Article history:
Received 31 August 2008
Received in revised form
18 November 2008
Accepted 18 November 2008
Available online 28 November 2008

Keywords:
Layered $Li_{1+x}(Mn_{1/3}Co_{1/3}Ni_{1/3})_{1-x}O_2$ oxides
Deintercalation
Transport properties
Lithium batteries

ABSTRACT

In this work structural and transport properties of layered $Li_{1+x}(Mn_{1/3}Co_{1/3}Ni_{1/3})_{1-x}O_2$ oxides ($x = 0$; 0.03; 0.06) prepared by a "soft chemistry" method are presented. The excessive lithium was found to significantly improve transport properties of the materials, a corresponding linear decrease of the unit cell parameters was observed. The electrical conductivity of $Li_{1.03}(Mn_{1/3}Co_{1/3}Ni_{1/3})_{0.97}O_2$ composition was high enough to use this material in a form of a pellet, without any additives, in lithium batteries and characterize structural and transport properties of deintercalated $Li_{1.03-y}(Mn_{1/3}Co_{1/3}Ni_{1/3})_{0.97}O_2$ compounds. For deintercalated samples a linear increase of the lattice parameter c together with a linear decrease of the parameter a with the increasing deintercalation degree occurred, but only up to 0.4–0.5 mol of extracted lithium. Further deintercalation showed a reversal of the trend. Electrical conductivity measurements performed of $Li_{1.03-y}(Mn_{1/3}Co_{1/3}Ni_{1/3})_{0.97}O_2$ samples ($y = 0.1$; 0.3; 0.5; 0.6) showed an ongoing improvement, almost two orders of magnitude, in relation to the starting composition. Additionally, OCV measurements, discharge characteristics and lithium diffusion coefficient measurements were performed for $Li/Li^+/Li_{1.03-y}(Mn_{1/3}Co_{1/3}Ni_{1/3})_{0.97}O_2$ cells.

© 2008 Elsevier B.V. All rights reserved.

1. Introduction

Nowadays most of commercial lithium ion batteries use $LiCoO_2$ as the cathode material. However, due to the high cost and toxic properties of $LiCoO_2$ many researchers focus their attention on a development of new cathode materials with better properties.

Recently, layered $LiNi_{1/3}Co_{1/3}Mn_{1/3}O_2$, proposed by Ohzuku and Makimura [1], and similar oxides are extensively investigated as a promising advanced cathode materials for lithium ion batteries [2–16]. $LiNi_{1/3}Co_{1/3}Mn_{1/3}O_2$ was found to exhibit a high rechargeable capacity and good charge–discharge rate capability which strongly depend on the synthesis procedure [17–21]. Additionally, materials with the excess of lithium possess better cyclability, thermal stability, and rate capability than the stoichiometric one [22–25]. However, if the excess of lithium is too big in $Li_{1+x}(Mn_{1/3}Co_{1/3}Ni_{1/3})_{1-x}O_2$, it would lead to a reduction of theoretical capacity, therefore it must be balanced. Further improvement of the electrochemical properties of this group of materials might be achieved by pre-conditioning of the cathode powders for instance using NH_3 [26] or initial activating charge above 4.5 V [27].

In the present study we focused on characterization of the structural and transport properties of $Li_{1+x}(Mn_{1/3}Co_{1/3}Ni_{1/3})_{1-x}O_2$ layered oxides prepared by the "soft chemistry" method. An enhanced electrical conductivity of $Li_{1.03}(Mn_{1/3}Co_{1/3}Ni_{1/3})_{0.97}O_2$ composition, comparing to the stoichiometric sample, allowed lithium deintercalation from the cathode pellets. We were able to characterize the structural and transport properties evolution as a function of lithium content for such prepared $Li_{1.03-y}(Mn_{1/3}Co_{1/3}Ni_{1/3})_{0.97}O_2$ materials.

2. Experimental

$Li_{1+x}(Mn_{1/3}Co_{1/3}Ni_{1/3})_{1-x}O_2$ oxides with $x = 0$; 0.03 and 0.06 were synthesized by the "soft chemistry" method with ammonia salt of ethylenediaminetetraacetic acid (EDTA) used as a complexing agent. The required amounts of Li_2CO_3 (POCh, p.p.a.), $C_4H_6MnO_4{\cdot}4H_2O$ (Fluka, p.p.a.), $Co(NO_3)_2{\cdot}6H_2O$ (POCh, p.p.a.), and $Ni(NO_3)_2{\cdot}6H_2O$ (Aldrich, p.p.a.) were put in a minimal amount of deionized water. While stirring the solution, $C_6H_8O_7{\cdot}H_2O$ was added to dissolve Li_2CO_3. Then, ammonia salt of EDTA was added to the mixture as a complexing agent. The obtained solutions were heated up in air in quartz evaporating dishes until all excessive water evaporated. A sol–gel transition was observed during the evaporation process. During further heating of the obtained gels, at temperatures exceeding 200 °C, a decomposition of nitrides was

* Corresponding author. Tel.: +48 126172026; fax: +48 126172522.
E-mail address: xi@agh.edu.pl (K. Świerczek).

0378-7753/$ – see front matter © 2008 Elsevier B.V. All rights reserved.
doi:10.1016/j.jpowsour.2008.11.088

observed. For higher temperatures (around 400 °C) a decomposition and oxidation of the remaining organic matrix took place, leaving a black colored, very fine grained precursor powder. The XRD analysis of the precursor powder showed almost completely amorphous state with no clearly defined diffraction peaks. The obtained precursor powders were thoroughly mixed in agate mortar, formed into pellets by uniaxial pressing at 100 MPa and heated at 800 °C in air for 1 h. This step was introduced in order to minimize the amount of residual carbon after EDTA and citric acid decomposition. After cooling to room temperature (RT) the samples were grounded in mortar, pressed uniaxially at 100 MPa into pellets of 13 mm diameter and about 1 mm thickness, and heated in air at 800 °C for 18 h and slowly cooled to room temperature. Second series of the samples was obtained by the same route, only with a different final heating, performed at 900 °C. The samples heated at 800 °C are named in this text as E800, while the ones obtained at 900 °C are named as E900. Relative density of the pellets was measured. The obtained values were about 80% for all of the samples, suggesting rather poor sinterability.

Crystal structure of the samples was characterized by the X-ray diffraction (XRD) using an X-ray diffractometer (Phillips X'Pert Pro) with CuK_α radiation. The measurements were performed in the 10–80° range. The X-ray patterns were analyzed using Rietveld method with RayFlex software. This structural analysis was supplemented with Scanning Electron Microscopy (SEM) and Energy Dispersive X-Ray Spectroscopy (EDX) studies.

Despite rather low relative density of the pellets it was possible to compare transport properties, as all of the pellets exhibited almost the same relative density. Nevertheless, in terms of the specific electrical conductivity an additional error can be expected. According to the simplified Bruggeman equation for samples with relative density equal 80%, the real values of the electrical conductivity are equal 1.43 times the measured ones. This corresponds to the relatively small correction equal +0.15 on the $\log\sigma$ scale. It must be noticed however that the activation energy of the electrical conductivity is generally not affected by this error, also, the thermoelectric power measurements are not affected as Seebeck coefficient is not related to the sample density or shape.

The electrical conductivity measurements were performed in air in RT–800 °C range by a pseudo-four probe DC method using platinum electrodes. Samples with cuboid shape of about 3 mm × 3 mm × 8 mm were used for the measurements.

The thermoelectric power measurements were carried out in air in 50–800 °C temperature range. Measurements were performed by means of a dynamic method. Two thermocouples were used to control temperature on both sides of the sample. An additional heater was used to heat up one side of the sample about 3–5°. A ten point dependence of the changes of the thermoelectric voltage as a function of temperature difference between both sides of the sample was measured. A liner regression was performed on the obtained data in order to calculate slope of the dependence, which gave value of the Seebeck coefficient. For thermoelectric power dependence as a function of temperature only points with linear correlation coefficient $R \geq 0.99$ were used.

In order to obtain deintercalated samples, $Li_{1.03}(Mn_{1/3}Co_{1/3}Ni_{1/3})_{0.97}O_2$ pellets weighing about 0.1 g were placed in $Li/Li^+/Li_{1.03-y}(Mn_{1/3}Co_{1/3}Ni_{1/3})_{0.97}O_2$ cells and charged up to desired lithium composition. 1 M solution of $LiClO_4$ in ethylene carbonate (EC)/dimethyl carbonate (DMC) electrolyte was used. Due to the relatively low electrical conductivity of the pellets and because no additives were used in the construction of the cell the used charge rates were low (10–20 $\mu A\,cm^{-2}$). Cell voltage during charge process was measured using a computer controlled amperostat Kest 32k. The maximum voltage was set at 4.6 V. After charging a relaxation process was introduced. Change smaller than 9 mV/24 h of the cell voltage was set as a criterion of the end of the relaxation. Before measuring transport properties, pellets were thoroughly rinsed in acetone and dried.

To evaluate electrochemical performance of $Li_{1.03}(Mn_{1/3}Co_{1/3}Ni_{1/3})_{0.97}O_2$ as the cathode material, the positive electrodes were prepared by mixing the obtained powders (75 wt.%) with polyvinilidene fluoride (10 wt.%) dissolved in N-methyl-2-pyrrolidone (NMP) together with carbon black (7.5 wt.%), and micrometric size graphite (7.5 wt.%). The obtained paste was spread on the surface of aluminum foil. Using such prepared cathode, metallic lithium anode, and 1 M $LiClO_4$ in EC/DMC electrolyte, the cells were assembled in a glove box filled with argon. Charge–discharge curves were measured using a computer controlled amperostat Kest 32k. A relatively fast C/3 rate was used. The voltage of the charge–discharge processes was set to be in the 2.5–4.6 V range. Lithium diffusion coefficient was measured by GITT technique and for some compositions by EIS technique. For impedance measurements Solartron 1252A FRA together with 1287 Electrochemical Interface were used. The obtained spectra were fitted using ZView software.

3. Results and discussion

3.1. Structure and microstructure

All of the obtained lithium–manganese–cobalt–nickel oxides from E800 and E900 series were single phased and possessed trigonal, $R\bar{3}m$, layered type crystal structure. Li^+/Ni^{2+} cation mixing was estimated not to exceed 3%. Unit cell parameters and calculated crystallite sizes are presented in Table 1. A linear decrease of *a* and *c* parameters with the increasing lithium excess was observed. A difference between E800 and E900 series is not significant and may be related to some lithium loss and a difference in oxygen nonstoichiometry which occur at higher temperatures.

It was reported that 3*d* metals in $LiMn_{1/3}Co_{1/3}Ni_{1/3}O_2$ have different oxidation states: Mn^{4+}, Co^{3+} and Ni^{2+} [28,29]. Also, it was found that the additional lithium present in these materials causes an oxidation of Ni^{2+} to Ni^{3+} [5,30]. Consequently, the results presented in Table 1 can be explained by taking into account the difference of the ionic radii between Ni^{2+} ions (0.69 Å), Ni^{3+} (low spin 0.56 Å) and Li^+ (0.76 Å). Due to the electroneutrality principle, one additional Li^+ ion causes the oxidation of two Ni^{2+} to Ni^{3+} ions and overall it leads to the shrinkage of the unit cell [24].

The calculated crystallite sizes presented in Table 1 show that the EDTA based synthesis yields sub-micron powders with E900 series having larger crystallite sizes than E800 series for all the compositions. With the excess of lithium a decrease of the crystallite size was observed for both series. Exemplary SEM images for $Li_{1.03}(Mn_{1/3}Co_{1/3}Ni_{1/3})_{0.97}O_2$ E800 and E900 samples are presented in Fig. 1. Similar agglomerates consisting of many smaller crystallites may be observed in both cases.

A distribution of 3*d* metals in the obtained materials was verified using EDX spectroscopy and was found to be homogenous for all of the samples.

3.2. Transport properties

High temperature electrical conductivity and thermoelectric power data are presented in Figs. 2 and 3. For both series of materials a significant difference in the electrical conductivity between the stoichiometric $LiMn_{1/3}Co_{1/3}Ni_{1/3}O_2$ and the samples with excess of lithium was observed. A large decrease of the activation energy from about 0.5–0.6 eV to about 0.3 eV and a substantial increase of the electrical conductivity was observed.

Extrapolating the high temperature electrical conductivity data for the stoichiometric compounds we estimated that the RT value is

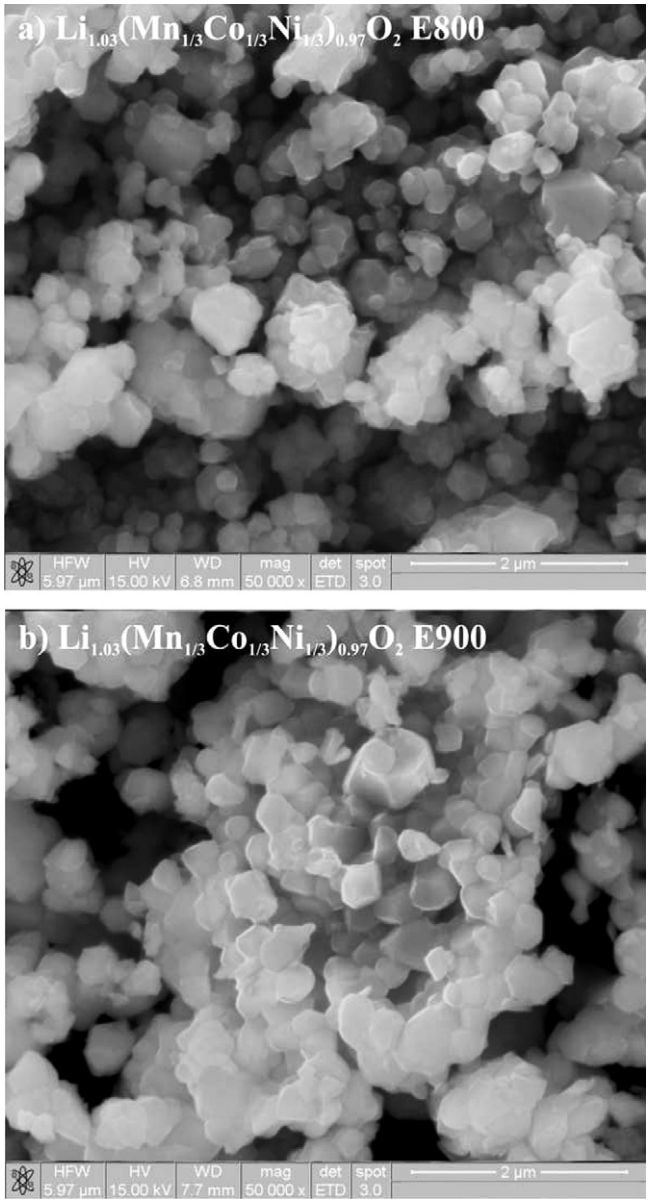

Fig. 1. SEM micrographs of (a) $Li_{1.03}(Mn_{1/3}Co_{1/3}Ni_{1/3})_{0.97}O_2$ E800 and (b) $Li_{1.03}(Mn_{1/3}Co_{1/3}Ni_{1/3})_{0.97}O_2$ E900 samples.

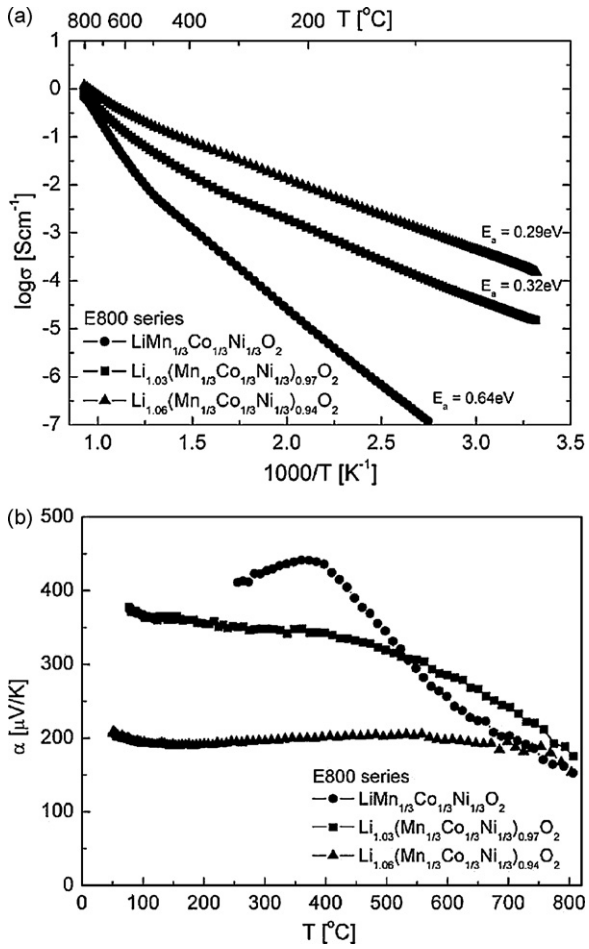

Fig. 2. Temperature dependence of (a) electrical conductivity and (b) thermoelectric power of $Li_{1+x}(Mn_{1/3}Co_{1/3}Ni_{1/3})_{1-x}O_2$ E800 samples at high temperatures. Activation energies E_a were calculated in the RT–400 °C range.

very low and is in the 10^{-8} S cm^{-1} range. For $LiMn_{1/3}Co_{1/3}Ni_{1/3}O_2$ oxide transition metal ions exhibit corresponding electronic configurations: Mn^{4+} $t_{2g}{}^3e_g{}^0$, low spin Co^{3+} $t_{2g}{}^6e_g{}^0$, Ni^{2+} $t_{2g}{}^6e_g{}^2$, so there are no free charge carriers, therefore no effective transport can take place. This would explain low electrical conductivity (Figs. 2a and 3a) and high, positive values of the thermoelectric power (Figs. 2b and 3b). Comparing to previous results for $LiCoO_2$ [31] and $LiNi_{1-y}Co_yO_2$ [32] one may notice several orders of magnitude lower electrical conductivity and higher activation energy for $LiMn_{1/3}Co_{1/3}Ni_{1/3}O_2$ material. Additionally for this sample the electrical conductivity was smaller comparing to previous report for $LiNi_{0.5-y}Mn_{0.5-y}Co_{2y}O_2$ series [33].

Lithium excess $x = 0.03$ caused a three orders of magnitude improvement of the electrical conductivity of the material, $Li_{1.03}(Mn_{1/3}Co_{1/3}Ni_{1/3})_{0.97}O_2$ samples possess the electrical conductivity at RT equal to about 10^{-5} S cm^{-1} (Figs. 2a and 3a). For $Li_{1.06}(Mn_{1/3}Co_{1/3}Ni_{1/3})_{0.94}O_2$ composition further increase of the electrical conductivity of about one order of magnitude was observed. The improvement of the transport properties of samples with lithium excess may be directly related to the appearance of the Ni^{3+} cations which allow hopping between Ni^{2+} and Ni^{3+}

Table 1
Lattice constants (in hexagonal setting) and crystallite size calculated from X-ray data for $Li_{1+x}(Mn_{1/3}Co_{1/3}Ni_{1/3})_{1-x}O_2$ samples.

Composition	E800		E900	
	Lattice constants [Å]	Crystallite size [nm]	Lattice constants [Å]	Crystallite size [nm]
$LiMn_{1/3}Co_{1/3}Ni_{1/3}O_2$	*a* 2.8628(1) *c* 14.2447(6)	105	*a* 2.8634(1) *c* 14.2460(4)	300
$Li_{1.03}(Mn_{1/3}Co_{1/3}Ni_{1/3})_{0.97}O_2$	*a* 2.8605(1) *c* 14.2292(9)	90	*a* 2.8618(1) *c* 14.2360(1)	210
$Li_{1.06}(Mn_{1/3}Co_{1/3}Ni_{1/3})_{0.94}O_2$	*a* 2.8587(2) *c* 14.2160(20)	70	*a* 2.8582(1) *c* 14.2232(1)	200

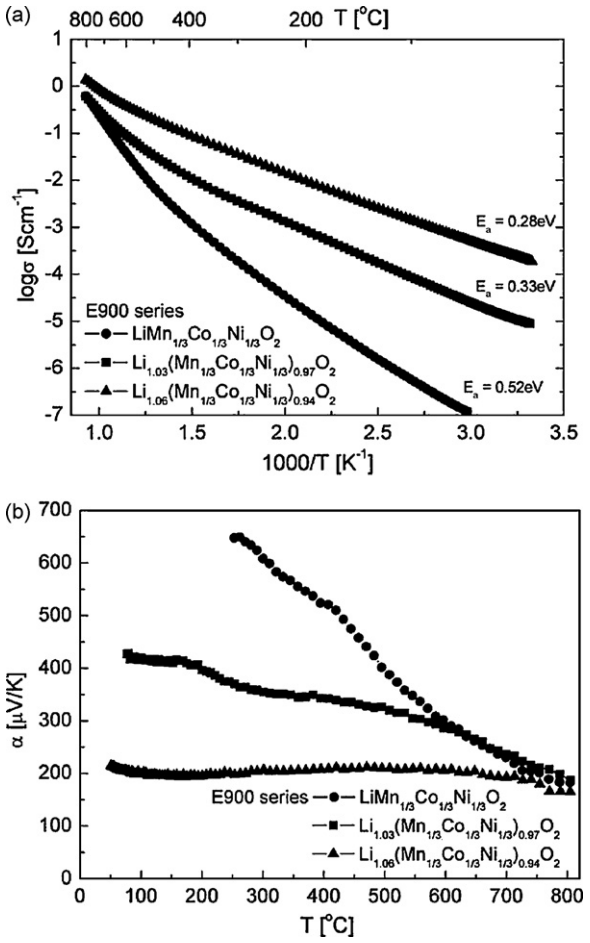

Fig. 3. Temperature dependence of (a) electrical conductivity and (b) thermoelectric power of $Li_{1+x}(Mn_{1/3}Co_{1/3}Ni_{1/3})_{1-x}O_2$ E900 samples at high temperatures. Activation energies E_a were calculated in the RT–400 °C range.

ions. Furthermore, a decrease of the unit cell *a* parameter, which may be related to the effectiveness of the 3*d* metal orbitals overlap, favors enhancement of the transport properties. Nevertheless, even the best conducting $Li_{1.06}(Mn_{1/3}Co_{1/3}Ni_{1/3})_{0.94}O_2$ samples possess lower conductivity than $LiCoO_2$ or $LiNi_{1-y}Co_yO_2$ compositions. Due to the electronic configuration of Mn^{4+} and Co^{3+} these cations do not participate in the charge transport at lower temperatures. Assuming perfect oxygen stoichiometry and oxidation states of Mn equal +4 and Co equal +3, in case of the $Li_{1.03}(Mn_{1/3}Co_{1/3}Ni_{1/3})_{0.97}O_2$ composition, the formal average oxidation state of Ni would increase to 2.19 and furthermore increase to 2.38 for the $Li_{1.06}(Mn_{1/3}Co_{1/3}Ni_{1/3})_{0.94}O_2$ composition. An effective charge transport between Ni^{2+} and Ni^{3+} in a narrow Ni e_g band states may be expected with higher values of the electrical conductivity and lower, but still positive, due to the dominance of the Ni^{2+} states, values of the Seebeck coefficient (Figs. 2b and 3b).

3.3. Structural and transport properties of deintercalated $Li_{1.03-y}(Mn_{1/3}Co_{1/3}Ni_{1/3})_{0.97}O_2$

In order to obtain deintercalated samples, $Li_{1.03}(Mn_{1/3}Co_{1/3}Ni_{1/3})_{0.97}O_2$ composition from E800 and E900 series were chosen, due to their better electrical conductivity as compared to the stoichiometric samples, and also because their theoretical capacity remains very high. We were able to use cathode pellets in lithium batteries, so open circuit voltage (OCV), structural and electrical measurements presented below

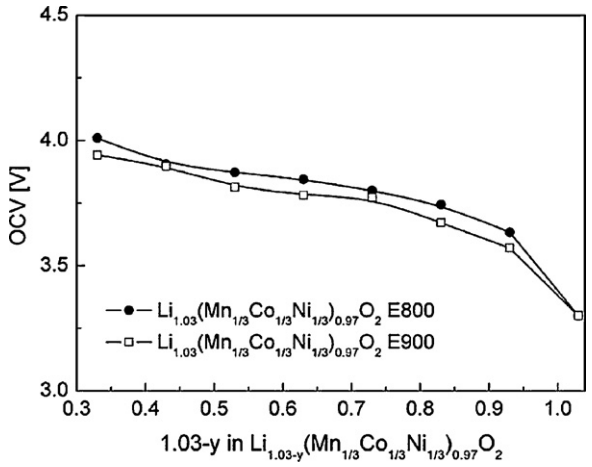

Fig. 4. Open circuit voltage of deintercalated $Li_{1.03-y}(Mn_{1/3}Co_{1/3}Ni_{1/3})_{0.97}O_2$ E800 and E900 pellets.

were performed on pure materials without any additives. Due to major problems with deintercalation of pellet sized samples the electrical conductivity measurements of deintercalated materials are not performed often. They require very long times of the deintercalation process with low current density and sufficient electrical conductivity of the cathode material in order to obtain homogenous samples suitable for measurements.

In Fig. 4 OCV data for $Li_{1.03-y}(Mn_{1/3}Co_{1/3}Ni_{1/3})_{0.97}O_2$ E800 and E900 samples as a function of lithium content in the $0 \le y \le 0.7$ range are presented. The monotonous character of OCV changes was observed. Such a behavior may be explained assuming that the electronic states of the oxidized 3*d* metals (Ni^{3+}, Ni^{4+} and Co^{4+}) create one effective energy band. Detailed analysis of the changes of the oxidation states for deintercalated $Li_{1-y}Mn_{1/3}Co_{1/3}Ni_{1/3}O_2$ was presented by Li et al. [34], which revealed that even for higher degrees of the deintercalation some amounts of Ni^{2+} and Co^{3+} remained in the material. The observed OCV for higher deintercalation degree is somewhat lower than reported in literature [35], suggesting some instability and oxygen loss from the samples [22]. The evolution of the unit cell parameters as a function of lithium content in $Li_{1.03-y}(Mn_{1/3}Co_{1/3}Ni_{1/3})_{0.97}O_2$ is presented in Fig. 5. A linear decrease of the *a* parameter and a corresponding increase of the *c* parameter during deintercalation can be noticed. This behavior was observed only up to 0.4–0.5 mol extracted of lithium. Further deintercalation in the measured range caused a decrease of the *c* parameter and the increase of the *a* parameter, more pronounced

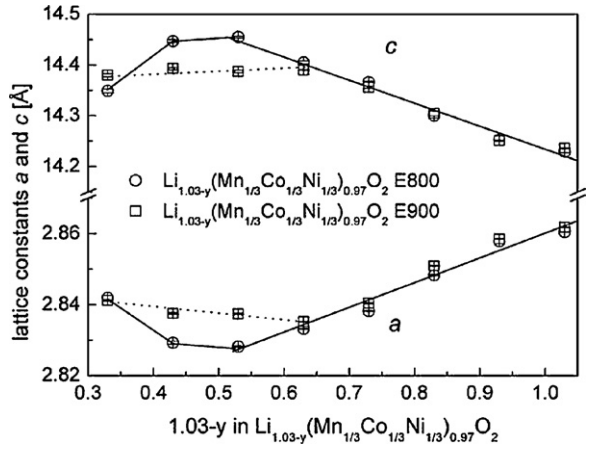

Fig. 5. Lattice constants evolution during deintercalation of $Li_{1.03-x}(Mn_{1/3}Co_{1/3}Ni_{1/3})_{0.97}O_2$ pellets.

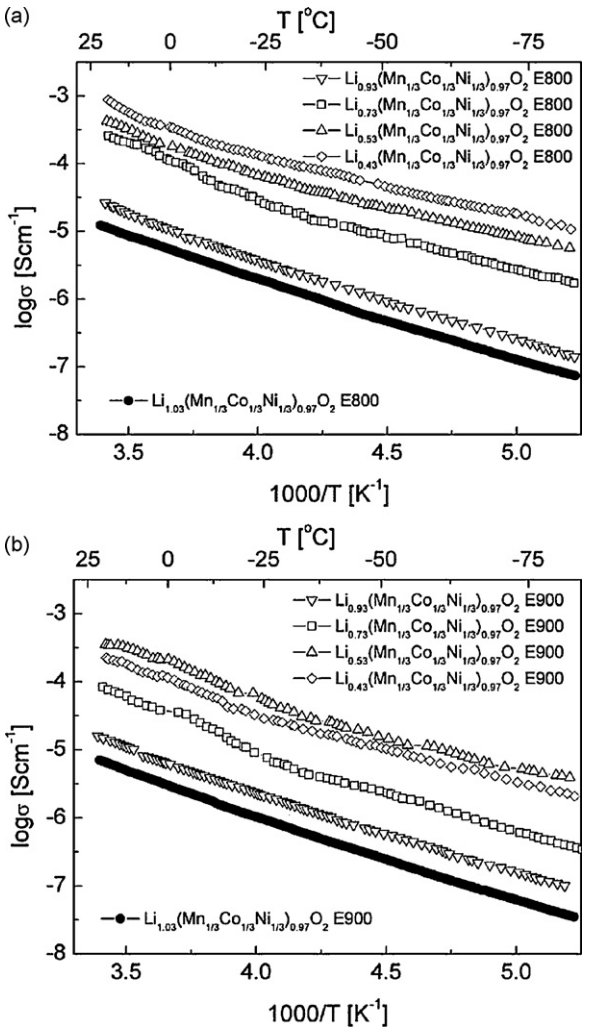

Fig. 6. Electrical conductivity of deintercalated $Li_{1.03-x}(Mn_{1/3}Co_{1/3}Ni_{1/3})_{0.97}O_2$ pellets from (a) E800 series and (b) E900 series.

in case of the E800 series. Similar data can be also found in the literature, however, there is some disagreement concerning the changes of the unit cell volume [6,21,22]. Our results seem to support data presented by Choi and Manthiram [22], but the calculated changes are smaller ($\Delta V/V_0 = 0.7\%$ for $y = 0.5$). The increase of the c constant initially may be correlated with the increasing oxidation state of 3d metals and therefore higher repulsion of layers. For higher deintercalation degree, the amount of lithium is insufficient to support layers. Therefore collapsing of the structure may be expected. The initial decrease of the a parameter could be connected to the smaller size of the oxidized 3d metal ions.

The temperature dependences of the electrical conductivity for deintercalated $Li_{1.03-y}(Mn_{1/3}Co_{1/3}Ni_{1/3})_{0.97}O_2$ samples, for $y = 0.1$; 0.3; 0.5 and 0.6, from both series are presented in Fig. 6a and b. Initially, for $y = 0.1$ the observed values of the electrical conductivity were only somewhat higher, comparing to the corresponding initial materials. For these compositions the formal oxidation state of Ni is equal to 2.50. Consequently, the observed increase of the electrical conductivity can be explained as a result of the increase of the charge carrier concentration, which is accompanied by the decrease of the 3d–3d metal distance (decrease of the a parameter). For samples with higher deintercalation degree ($y = 0.3$; 0.5 and 0.6) further increase of the electrical conductivity of about 1–2 orders of magnitude was observed (Fig. 6a and b).

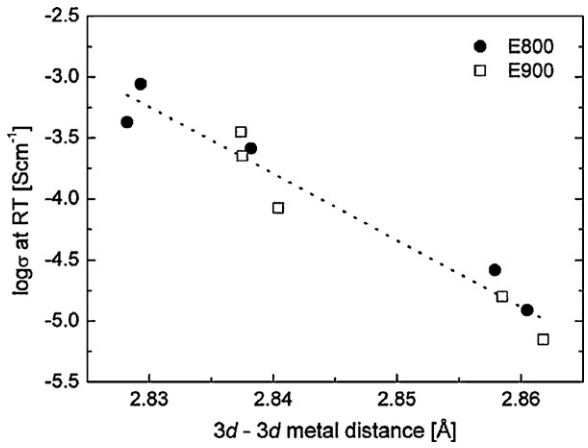

Fig. 7. RT dependence of the electrical conductivity as a function of the 3d–3d metal distance for initial $Li_{1.03}(Mn_{1/3}Co_{1/3}Ni_{1/3})_{0.97}O_2$ and deintercalated samples.

The observed increase of the electrical conductivity could be associated with the appearance of additional Ni^{4+} and Co^{4+} cations created by lithium removal during deintercalation, which allow for additional hopping between 3d sites and with further decrease of the a parameter. While the decrease of the 3d–3d metal distance observed during deintercalation is quite significant, the observed values are too high for the insulator–metal transition to appear. A semi-empirical parameter R_C, calculated according to Goodenough's equation [36], for which insulator–metal transition occurs is equal to 2.845 Å for the $Li_{1.03}(Mn_{1/3}Co_{1/3}Ni_{1/3})_{0.97}O_2$ composition. It is a smaller value than the actual distance between 3d cations (2.86 Å). During deintercalation the actual distance between 3d cations decreases, but also the R_C decreases due to the changes in the average oxidation state of transition metals accompanied by changes of the average spin state. The actual 3d–3d metal distance remains always above the critical R_C and no insulator–metal transition occurs. For comparison, in case of Li_xCoO_2 such insulator–metal transition was observed [31], with R_C being a good qualitative parameter describing it.

Fig. 7 shows values of the electrical conductivity for starting $Li_{1.03}(Mn_{1/3}Co_{1/3}Ni_{1/3})_{0.97}O_2$ and deintercalated samples as a function of the 3d–3d metal distance. The observed dependence for both series of materials is quite linear. This means that the 3d–3d metal distance plays an important role in the transport properties. Surprisingly, the increase of the electrical conductivity is not correlated with a decrease of the activation energy (Fig. 6a and b). The activation energy of the electrical conductivity remains almost the same for all deintercalated samples. Additional studies are needed to explain this result.

The observed increase of the electrical conductivity of the deintercalated samples may be beneficial in terms of the application of these materials. It would improve macroscopic, charge distribution over the cathode material.

3.4. Electrochemical properties

The lithium diffusion coefficient as a function of the deintercalation degree in the cathode material was measured by GITT method and for some compositions using EIS technique. Detailed discussion of the procedures applied to this type of materials was presented by Shaju et al. [35]. As shown in Fig. 8, the values of D_{Li} remain in the 5×10^{-11} to 10^{-9} cm^2 s^{-1} range for both series of the materials. No significant dependence of D_{Li} as a function of lithium content was observed. The data from EIS measurements for $Li_{1.03-y}(Mn_{1/3}Co_{1/3}Ni_{1/3})_{0.97}O_2$ E900 well matches the values obtained by GITT method. Due to some uncertainty about

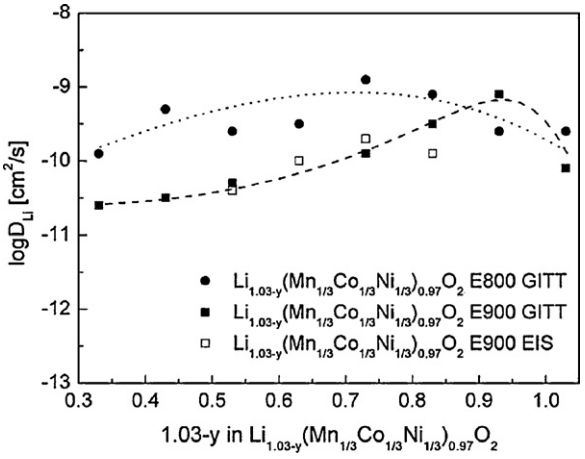

Fig. 8. Lithium diffusion coefficient as a function of lithium concentration for $Li_{1.03-y}(Mn_{1/3}Co_{1/3}Ni_{1/3})_{0.97}O_2$ E800 and E900 series.

an assumption of the contact area between the cathode material and the electrolyte, the values of the lithium diffusion coefficient for both series of materials can be considered to be the same within the error range. Similar values of D_{Li} were reported previously for $Li_{1-y}Mn_{1/3}Co_{1/3}Ni_{1/3}O_2$ [35].

The intercalation process can be described as an ambipolar diffusion of lithium and electrons. In case of Li_xCoO_2 a close correlation between the electrical conductivity and the lithium diffusion coefficient was proved [31]. Despite rather significant increase of the electrical conductivity for deintercalated $Li_{1.03-y}(Mn_{1/3}Co_{1/3}Ni_{1/3})_{0.97}O_2$ samples (Fig. 6a and b), values of the lithium diffusion coefficient remain almost constant in the whole range (Fig. 8). The observed results suggest that the electronic transport in the case of $Li_{1.03-y}(Mn_{1/3}Co_{1/3}Ni_{1/3})_{0.97}O_2$ samples is not the limiting factor for lithium movement.

In Fig. 9 preliminary data regarding discharge characteristics of $Li/Li^+/Li_{1.03-y}(Mn_{1/3}Co_{1/3}Ni_{1/3})_{0.97}O_2$ cells are presented. In both cases (E800 and E900 cathode materials) the discharge was performed at C/3 rate down to 2.5 V. Initially, the cells were charged up to 4.6 V. On the contrary to the E800 material, which performed rather poorly, the curves obtained for $Li_{1.03-y}(Mn_{1/3}Co_{1/3}Ni_{1/3})_{0.97}O_2$ E900 cathodes are quite promising. The observed capacity in both discharges exceeded 175 mAh g^{-1}. This major difference between these materials can be only attributed to the different crystalline sizes (Table 1), as structural and transport properties of both $Li_{1.03}(Mn_{1/3}Co_{1/3}Ni_{1/3})_{0.97}O_2$ compounds were almost the same. It seems, that the microstructure of the cathode material is crucial in terms of the actual performance in lithium cells, with grain size being important parameter, which needs to be optimized.

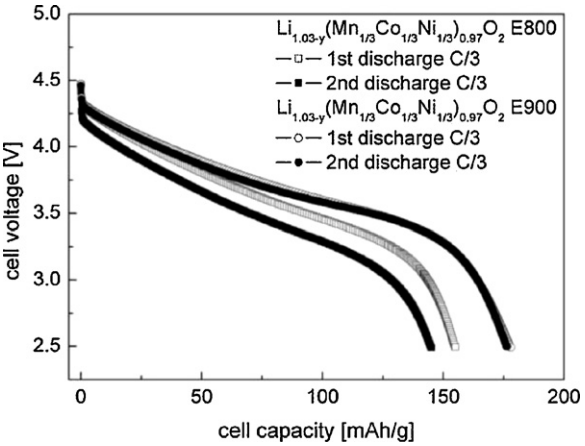

Fig. 9. First two discharge curves of $Li/Li^+/Li_{1.03-y}(Mn_{1/3}Co_{1/3}Ni_{1/3})_{0.97}O_2$ cells performed at C/3 rate.

4. Conclusions

The presented soft chemistry EDTA based method was successfully applied for obtaining layered $Li_{1+x}(Mn_{1/3}Co_{1/3}Ni_{1/3})_{1-x}O_2$ oxides. The excess of lithium caused the linear decrease of the unit cell parameters. Additional Ni^{3+} present in the samples with the excess of lithium improved their transport properties. It was possible to measure OCV, structural and transport properties on deintercalated $Li_{1.03-y}(Mn_{1/3}Co_{1/3}Ni_{1/3})_{0.97}O_2$ pellets ($y = 0.1$; 0.3; 0.5 and 0.6). Deintercalation of lithium was found to cause the linear decrease of the *a* parameter and the increase of the *c* parameter of the unit cell, but only up to 0.4–0.5 mol of extracted lithium. The improvement of the electrical conductivity for deintercalated samples was quite significant and it can be attributed to the increasing amounts of Ni^{3+}, Ni^{4+} and Co^{4+} cations and to the decreasing *a* parameter. Lithium diffusion coefficient as a function of deintercalation degree was measured for $Li_{1.03-y}(Mn_{1/3}Co_{1/3}Ni_{1/3})_{0.97}O_2$ samples and was found to be in the 5×10^{-11} to 10^{-9} cm^2 s^{-1} range.

Acknowledgments

This work was partially supported by Polish Ministry of Science and Higher Education under Singapore-Poland Joint Research Project nr SINGAPUR/99/2007.

This work was partially supported by the European Commission (project *Dev-BIOSOFC*, FP6-042436, MTKD-CT-2006-042436).

References

[1] T. Ohzuku, Y. Makimura, Chem. Lett. 30 (7) (2001) 642.
[2] P. He, H. Wang, L. Qi, T. Osaka, J. Power Sources 160 (2006) 627.
[3] S. Zhang, X. Qiu, Z. He, D. Weng, W. Zhu, J. Power Sources 153 (2006) 350.
[4] J. Choi, A. Manthiram, Electorochem. Solid-State Lett. 8 (2005) C102.
[5] N. Tran, L. Croguennec, C. Labrugere, C. Jordy, P. Biensan, C. Delmas, J. Electrochem. Soc. 153 (2006) A261.
[6] N. Yabuuchi, T. Ohzuku, J. Power Sources 119–121 (2003) 171.
[7] I. Saadoune, M. Dahbi, M. Wikberg, T. Gustafsson, P. Svedlindh, K. Edström, Solid State Ionics 178 (2008) 1668.
[8] T.A. Arunkumar, E. Alvarez, A. Manthiram, J. Electrochem. Soc. 154 (2007) A770.
[9] S.-T. Myung, A. Ogata, K.-S. Lee, S. Komaba, Y.-K. Sun, H. Yashiro, J. Electrochem. Soc. 155 (5) (2008) A374.
[10] M. Ma, N.A. Chernova, B.H. Toby, P.Y. Zavalij, M.S. Whittingham, J. Power Sources 165 (2007) 517.
[11] Z. Lu, D.D. MacNeil, J.R. Dahn, Electorochem. Solid-State Lett. 4 (11) (2001) A191.
[12] Z. Lu, D.D. MacNeil, J.R. Dahn, Electorochem. Solid-State Lett. 4 (12) (2001) A200.
[13] Z. Lu, L.Y. Beaulieu, R.A. Donaberger, C.L. Thomas, J.R. Dahn, J. Electrochem. Soc. 149 (6) (2002) A778.
[14] D.D. MacNeil, Z. Lu, J.R. Dahn, J. Electrochem. Soc. 149 (10) (2002) A1332.
[15] S. Jouanneau, J. Jiang, K.W. Eberman, L.J. Krause, J.R. Dahn, J. Electrochem. Soc. 150 (12) (2003) A1637.
[16] K.W. Eberman, L.J. Krause, J.R. Dahn, J. Electrochem. Soc. 152 (9) (2005) A1879.
[17] L. Zhang, X. Wang, T. Muta, D. Li, H. Noguchi, M. Yoshio, R. Ma, K. Takada, T. Sasaki, J. Power Sources 162 (2006) 629.
[18] X. Li, Y.J. Wei, H. Ehrenberg, F. Du, C.Z. Wang, G. Chen, Solid State Ionics 178 (2008) 1969.
[19] H. Ren, Y. Wang, D. Li, L. Ren, Z. Peng, Y. Zhou, J. Power Sources 178 (2008) 439.
[20] B. Lin, Z. Wen, Z. Gu, S. Huang, J. Power Sources 175 (2008) 564.
[21] N. Yabuuchi, Y. Makimura, T. Ohzuku, J. Electrochem. Soc. 154 (2007) A314.
[22] J. Choi, A. Manthiram, Electrochem. Solid-State Lett. 7 (2004) A365.
[23] Y.M. Todorov, K. Numata, Electrochim. Acta 50 (2004) 495.
[24] J.-M. Kim, N. Kumagai, Y. Kadoma, H. Yashiro, J. Power Sources 174 (2007) 473.
[25] S.-H. Park, S.-H. Kang, I. Belharouak, Y.K. Sun, K. Amine, J. Power Sources 177 (2008) 177.
[26] J.-S. Kim, C.S. Johnson, J.T. Vaughey, M.M. Thackeray, J. Power Sources 153 (2006) 258.
[27] Z. Lu, J.R. Dahn, J. Electrochem. Soc. 149 (7) (2002) A815.
[28] B.J. Hwang, Y.W. Tsai, D. Carlier, G. Ceder, Chem. Mater. 15 (2003) 3676.
[29] H. Kobayashi, Y. Arachi, S. Emura, H. Kageyama, K. Tatsumi, T. Kamiyama, J. Power Sources 146 (2005) 640.

[30] K. Shizuka, T. Kobayashi, K. Okahara, K. Okamoto, S. Kanzaki, R. Kanno, J. Power Sources 146 (2005) 589.
[31] J. Molenda, A. Stokłosa, T. Bąk, Solid State Ionics 36 (1989) 53.
[32] P. Wilk, J. Marzec, J. Molenda, Solid State Ionics 157 (2003) 109.
[33] J. Choi, A. Manthiram, Solid State Ionics 176 (2005) 2251.
[34] J. Li, Z.R. Zhang, X.J. Guo, Y. Yang, Solid State Ionics 177 (2006) 1509.
[35] K.M. Shaju, G.V. Subba Rao, B.V.R. Chowdari, J. Electrochem. Soc. 151 (2004) A1324.
[36] J.B. Goodenough, in: H. Reiss (Ed.), Progress in Solid State Chemistry, vol. 5, Pergamon Press, Oxford, 1971, p. 279.